High precision NH_3 sensing using network nano-sheet Co_3O_4 arrays based sensor at room temperature

Zhijie Li[1], Zhijie Lin[1], Ningning Wang[1], Junqiang Wang[1], Wei Liu[1], Kai Sun[2], Yong Qing Fu[3*], Zhiguo Wang[1*]

[1]School of Physical Electronics, University of Electronic Science and Technology of China, Chengdu 610054, PR China
[2]Department of Nuclear Engineering and Radiological Sciences, University of Michigan, Ann Arbor, MI 48109-2104, USA
[3]Department of Physics and Electrical Engineering, Faculty of Engineering and Environment, Northumbria University, Newcastle Upon Tyne NE1 8ST, England, United Kingdom

* Corresponding author. Tel.: +86 02883200728. E-mail address: zgwang@uestc.edu.cn (Zhiguo Wang); Richard.fu@northumbria.ac.uk (Richard Yong Qing Fu)

Abstract

Network nano-sheet arrays of Co_3O_4 for high precision NH_3 sensing application were prepared on alumina tube using a facile hydrothermal process without template or surfactant, and their morphology, nanostructures and NH_3 gas sensing performance were investigated. The prepared nano-sheet Co_3O_4 arrays showed a network structure with an average sheet thickness of 39.5 nm. Detailed structural analysis confirmed that the synthesized Co_3O_4 nano-sheets were consisted of nanoparticles with an average diameter of 20.0 nm. NH_3 gas sensor based on these network Co_3O_4 nano-sheet arrays showed a low detection limit (0.2 ppm), rapid response/recovery time (9 s/134 s for 0.2 ppm NH_3), good reproducibility and long-term stability for NH_3 detection at room temperature.

Keywords: Co_3O_4; Nano-sheet array; Hydrothermal; NH_3 gas; Gas sensor

1. Introduction

Recently there is a huge demand for monitoring and controlling air pollutants, in which ammonia (NH_3) is one of the most common ones causing severe environmental problems. The search for new and more effective solid state chemical sensors for monitoring low level concentrations of ammonia in air is of great interest in many fields, including automotive, industrial process monitoring, medical diagnostics and air quality control. One of the mostly used sensing mechanisms for the NH_3 is based on resistive sensors using various metal oxide semiconductors [1,2], such as ZnO [3-4], WO_3 [5], In_2O_3 [6-7], ZrO_2 [8], V_2O_5 [9], carbon nanotubes [10-11], Fe_2O_3 [12] and Co_3O_4 [13]. Among these, cobalt oxide, Co_3O_4, has received much research attention due to its high resistance to corrosion, abundant raw material and non-toxicity. It is a promising material for applications in Li-ion batteries [14-16], catalysts [17,18], and gas sensors [13,19-25]. In particular, the oxidative catalytic activity of the Co_3O_4 is superior [17], thus it can be directly used to design or enhance the gas response, selectivity, and sensing kinetics [13,19-25]. However, most reports on the Co_3O_4 sensors [13,19-21,24,25] were focused on high temperature sensing applications (i.e., up to 300 ^oC). Up to now, the NH_3 sensor based on the Co_3O_4 operated at room temperature has not been reported.

As we know, the dimensionality, size and morphology of the oxide nanostructures have significant influences to their physical and chemical properties. Development of novel nanostructured transitional metal oxides with controlled shapes and morphologies has stimulated considerable research interest due to their novel physical

and chemical properties and potential wide-range applications [26-28]. So far, various morphological nanostructures of Co_3O_4 have been explored, including nanoparticles [19], nanofiber [20], nanowires [17,29-31], nanotube [15,16], nanobelt [32], nanorods [13,23,24], and nano-sheets [18,33,34] using various methods including thermal oxidation, hydrothermal synthesis, electrospinning and inverse microemulsion. Co_3O_4 nano-sheets grown directly on substrates should have excellent sensing performance because the interconnected nano-sheets will form a network porous nanoscale system which facilitates a fast and effective gas adsorption onto the entire sensing surface, thus significantly improving sensitivity and reducing the response time. However, development of low cost, large scale, highly sensitive and extremely selective gas sensors based on the Co_3O_4 nano-sheets grown directly on substrates still face many technical and economical challenges.

In this paper, a high precision NH_3 gas sensor operated at room temperature based on the Co_3O_4 nano-sheets grown directly on an alumina tube was reported using a facile hydrothermal method without any template or surfactant. The sensing characteristics including sensitivity, selectivity, stability, response time and recovery time as well as the NH_3 sensing mechanism based on the Co_3O_4 nano-sheets were investigated.

2. Experimental procedures

2.1 Materials synthesis and characterization

In a typical synthesis process, $Co(NO_3)_2 \cdot 6H_2O$ of 8.109 g, urea of 0.450 g and NH_4F of 0.111 g were dissolved into the distilled water of 80 ml under continuous

stirring at room temperature to form a homogeneous solution. Subsequently the obtained solution was transferred into a Teflon-lined stainless steel autoclave of 150 ml, and an alumina tube was placed vertically at the bottom of the autoclave. The autoclave was kept at 130 ^{o}C for 9 hours, and subsequently was cooled down to room temperature naturally. The resultant black precipitates of $Co(CO_3)_{0.5}(OH)\cdot 0.11H_2O$ was collected and washed with distilled water and absolute ethanol for three times, respectively. Then they were dried at 110 ^{o}C in air for two hours. Finally, the ceramic tube with the resultant black precipitate was annealed at 350 ^{o}C for two hours in air in order to obtain the black Co_3O_4.

Crystalline structures and phase composition of the Co_3O_4 nano-sheets were characterized using X-ray diffraction (XRD, Rigaku D/max-2500) with Cu Kα radiation at a wavelength of 1.5406 Å and operating voltage/current of 40 kV/30 mA. The morphologies of the obtained Co_3O_4 were observed using a scanning electron microscope (SEM, Inspect F50, USA) with an operation voltage of 5 kV. Transmission electron microscope (TEM, JEM-2200FS, Japan) was used to characterize crystallographic features of the sample. Surface porosity was characterized using a nitrogen physisorption apparatus (BELSORP-miniII, Japan) at 77.4 K. Before the measurements, the samples were degassed at 200 °C in a vacuum (with a based vacuum of 10^{-6} Pa) for 6 hours. The specific surface area was calculated by Brunauer–Emmett–Teller (BET) method. The total pore volumes (V_{total}) were evaluated from the adsorbed amounts of nitrogen at a relative pressure P/P_0 of 0.99. The pore size distribution was attained by the non-local density functional theory

(NLDFT) method. X-ray photoelectron spectroscopy (XPS, KratosAxis-Ultra DLD, Japan) was used with a monochromatic Al Kα radiation (1486.6 eV) in order to identify the chemical binding of the elements. UV–vis spectroscopy was recorded using a UV-2101 spectrophotometer (Shimadzu Corporation, Japan).

2.2 Gas sensor fabrication and measurements

The alumina tube coated with the Co_3O_4 nano-sheets was used to fabricate the sensors directly. A schematic diagram of the sensor design is shown in Fig. 1a. There are a pair of gold electrodes connected with Pt wires at each end of the ceramic tube. Between the two gold electrodes, it was the area coated with the Co_3O_4 nano-sheets film. A Ni-Cr heating wire was used as the heating supply source and was inserted inside the ceramic tube to control the operation temperature of the gas sensor.

Gas-sensing performance of the device was evaluated using a WS-30A gas sensor measurement system (Weisen Electronic Technology Co., Ltd., Zhengzhou, China). Fig.1b illustrates the measurement circuit of the gas sensor, where R_F is a load resistor connected in series with the gas sensor and R_S donates a resistor of the sensor. During testing, an appropriate working voltage ($V_{working}$=0.10 V in this study) was applied. The response of the gas sensor was monitored by the voltage changes of the R_F. The gas response (S) of the sensor was defined as follows: $S=R_g/R_a$ for the NH_3 gas, where the R_g and R_a are the electrical resistance of the sensor measured in the NH_3 gas and dry air, respectively.

3. Results and discussions

3.1 Structural and morphological characteristics

Fig. 2 shows the XRD spectra of the synthesized products before and after calcination. Before calcination, as shown in Fig. 2a, all of the diffraction peaks can be indexed to orthorhombic $Co(CO_3)_{0.5}(OH)\cdot 0.11H_2O$ (a = 8.792 Å, b = 10.150 Å and c = 4.433 Å; JCPDS No. 048-0083). The $Co(CO_3)_{0.5}(OH)\cdot 0.11H_2O$ has a layered structure and consists of positively charged Co-OH layers and counter anions located between the Co-OH layers, which can be easily converted into the Co_3O_4 [35]. The crystalline structure of the product was changed after it was annealed at 350 ^oC for 2 hours in air. All the diffraction peaks as shown in Fig. 2b can be indexed to spinel Co_3O_4 (JCPDS No. 42-1467) with the calculated lattice parameters of 8.084 Å. No other peaks of impurities are observed, indicating that the cobalt carbonate hydroxide precursor was completely transformed into crystalline Co_3O_4 after the calcination. Furthermore, the crystal size of the Co_3O_4 was estimated to be 20.0 nm according to the standard Scherrer formula:

$$L = K\lambda/\cos\theta \qquad (1)$$

where λ is the wavelength of the X-ray radiation (0.15406 nm for CuKα); K is a constant taken as 0.89; β is the line width at half maximum height and θ is the diffracting angle.

Fig. 3 presents typical SEM and TEM images of the network nano-sheet Co_3O_4 arrays. It can be seen from Fig. 3a and (b) that the Co_3O_4 nano-sheets have an average thickness of 39.5 nm, grown uniformly on the alumina tube. The thickness of the

nano-sheet Co_3O_4 arrays on alumina tube is 5.2 μm. The nano-sheet structure looks like maple leaves with one layer structure. Most of the nano-sheets are grown perpendicularly to the substrate surface, forming a network-like structure with cavities between the adjacent sheets. Naturally, these nano-sheets present a large effective area, leading to a significant enhancement of the target gas activities. A fraction of the nano-sheet was analyzed using TEM analysis and the results are shown in Fig. 3c. The as-synthesized nano-sheets consist of nanoparticles with an average diameter of 20.0 nm, which is consistent with the calculation results from the XRD analysis. High resolution TEM (HRTEM) image (Fig. 3d) shows a well-defined crystalline structure with an average lattice spacing of 0.243 nm corresponding to the value of the (311) planes of the Co_3O_4 phase.

The pore distribution curve of the nano-sheet Co_3O_4 sample is shown in Fig. 4. It can be found that the nano-sheet Co_3O_4 nanostructures have a mesoporous structure, with an average pores diameter of 16.39 nm and the total pore volumes of 0.3526 cm^3/g. The specific surface area obtained using the BET method for this sample is 61.69 $m^2 \cdot g^{-1}$.

On the basis of these characterization results and previous literature related to cobalt hydroxide-carbonate nanoparticles [35], we proposed a possible formation mechanism of the $Co(CO_3)_{0.5}(OH) \cdot 0.11H_2O$ precursors. At the beginning of the hydrothermal reactions, Co^{2+} ions were coordinated with F^- ions to form $CoFx^{(x-2)-}$ complexes in the homogeneous solution. After the temperature of the reactant solution was increased to 130 °C, the hydrolysis process of the urea took place and a number

of CO_3^{2-} and OH^- anions were formed gradually, which could help to release Co^{2+} ions from the $CoF_x^{(x-2)-}$ complexes. As a result, the CO_3^{2-} reacted with OH^- and $CoF_x^{(x-2)-}$ to form cobalt–hydroxide–carbonate precursors [31]. All the involved chemical reactions are based on the following formulas:

$$Co^{2+} + xF^- \rightarrow CoF_x^{(x-2)-} \quad (2)$$

$$H_2NCONH_2 + H_2O \rightarrow 2NH_3 + CO_2 \quad (3)$$

$$CO_2 + H_2O \rightarrow CO_3^{2-} + 2H^+ \quad (4)$$

$$NH_3 \cdot H_2O \rightarrow NH_4^+ + OH^- \quad (5)$$

$$CoF_x^{(x-2)-} + 0.5\ CO_3^{2-} + OH^- + 0.11H_2O \rightarrow Co(CO_3)_{0.5}(OH)\cdot 0.11H_2O + xF^- \quad (6)$$

The heat treatment stage at 350 ^oC was mainly associated with the decomposition of the $Co(CO_3)_{0.5}(OH)\cdot 0.11H_2O$ precursors and thermal formation of the Co_3O_4, which can be explained using the following formula:

$$6Co(CO_3)_{0.5}(OH)\cdot 0.11H_2O + O_2 \rightarrow 2Co_3O_4 + 3.11\ H_2O + 3CO_2 \quad (7)$$

Chemical states of the samples were analyzed using the XPS. Fig. 5 shows the XPS spectra of Co 2p and O 1s for the Co_3O_4. The binding energy data obtained from the XPS analysis are calibrated for specimen charging by referencing the C1s peak to 284.80 eV. As indicated in Fig. 5a, two major peaks are obtained which are centered at 780.18 and 795.93 eV, corresponding to the binding energies of the Co $2p_{3/2}$ and Co $2p_{1/2}$, respectively, with a spin orbit splitting of 15.0 eV, agreed with the previous reports [24,25, 36]. The asymmetric O 1s peak in the surface can be fitted with three nearly Gaussian components, centered at 530.09, 531.63 and 532.90 eV, respectively, as shown in Fig. 5b. The first peak at the low binding energy side of 530.09 eV is

attributed to the O^{2-} ions in the Co_3O_4 which are surrounded by Co atoms. Whereas the peaks located at the higher binding energy values of 531.63 eV and 532.90 eV can be assigned to oxygen species in adsorbed Co-OH and H_2O molecules, respectively [37].

Co_3O_4 is a p-type semiconductor and its optical band gap is strongly influenced by the size, shape, and dimensions of its crystals. Fig. 6a shows the UV-vis absorbance spectrum of the Co_3O_4 nano-sheets. There are three broad absorption bands centered at 245 nm, 456 nm and 759 nm, respectively, which are consistent with the published reports on the optical properties for the spinel type Co_3O_4 thin films [38]. The band gap Eg can be calculated from the following equation:

$$(\alpha h\nu)^n = A(h\nu - E_g) \qquad (8)$$

where $h\nu$ is the photon energy, α is the absorption coefficient, A is a constant characteristic to the material, E_g is the band gap, and n equals either 1/2 for an indirect transition, or 2 for a direct transition. The calculated $(\alpha h\nu)^2$ versus $h\nu$ curve is shown in Fig. 6b. The value of $h\nu$ extrapolated to α=0 gives the absorption band gap energy. The curve in Fig. 6b can be linearly fitted into 2 lines with the intercepts at 2.46 eV and 1.80 eV. As has been reported in the literature [39-40], the larger band gap of 2.46 eV should be associated with the $O^{-II} \rightarrow Co^{II}$ charge transfer process (basic optical band gap energy or valence to conduction band excitation), whereas the band gap of 1.80 eV should be related to the $O^{-II} \rightarrow Co^{III}$ charge transfer (with Co^{III} located below the conduction band). The best fitting of Eq. (8) to the absorption spectrum of the product gives n=2, which suggests that the as-synthesized Co_3O_4 nanocrystals are

semiconducting with a direct transition at these energies.

3.2 Gas sensing properties

The gas sensing performance of the sensors based on Co_3O_4 nano-sheets was characterized. Fig. 7 plots typical current-voltage (I-V) curves between the two neighboring platinum electrodes bridged by the Co_3O_4 nano-sheets at room temperature. The currents are increased linearly with the applied bias voltage (from -9 V to 9 V), indicating that good ohmic contacts are established between the Co_3O_4 nano-sheets layer and electrodes.

The response and recovery behaviors of the gas sensor operated at room temperature were investigated using different concentrations of the NH_3 gas, and the results are shown in Fig. 8a. It can be seen that the response is increased with increasing NH_3 concentration. Even at a low NH_3 concentration of 0.2 ppm, the Co_3O_4 nano-sheet based sensor still shows a good response. The electrical resistance values of the sensor quickly decrease as soon as the NH_3 gas are injected into chamber and then quickly recover to its initial values once the test chamber is refreshed with dry air, indicating the good repeatability and reversibility of the NH_3 sensor. The operating temperature is one of important sensing properties of a gas sensor and a low operating temperature such as room temperature in this study is preferable for its practical applications.

The response sensitivity of the Co_3O_4 nano-sheets sensor to the NH_3 (0.2–100 ppm) was calculated and the results are shown in Fig. 8b. The response sensitivity of the sensor increases with the concentration of the NH_3, but the sensor still has a good

response to the concentration as low as 0.2 ppm. A linear plot between the increase of the sensitivity and NH_3 concentration is obtained with the dynamic detection range from 1 ppm to 100 ppm as shown in Fig. 8b, revealing that the sensor presents a good linearity characteristic to the detection of NH_3. The equation fitted for the response sensitivity (S) and NH_3 concentration (C_{NH3}) was obtained based on the data in Fig. 8b:

$$S = 0.0819\ C_{NH3}+1.09128 \qquad (9)$$

Where S is the response sensitivity, C_{NH3} is the NH_3 concentration (in ppm). The constant of 0.0819 (in ppm^{-1}) and 1.09128 are the slope and altitude intercept of the fitted line.

Fig. 9 shows the response time and recovery time of the Co_3O_4 nano-sheets based sensor as a function of NH_3 concentration. The time resolution is 1 s. Here, the response time and recovery time are defined as the time to reach 90% of the maximum sensing response upon injection of the NH_3 gas and the time to fall to 10% of the maximum sensing response upon air purging. As can be seen from Fig. 9, the response time and recovery time show variations upon exposure to different concentrations of the NH_3 gas. The response time and recovery time are obviously shorter at lower concentrations of the NH_3 (i.e., less than 1 ppm) than those at higher concentrations (i.e., more than 1 ppm). For the 0.2 ppm NH_3, the senor shows fast response and recovery, and the response time and recovery time are only 9 s and 134 s, respectively.

Most reports on the NH_3 sensors [3,9,13] were focused on high temperature sensing

applications, whereas the NH_3 sensors applied to room temperature are quite limited. For example, Zeng et al reported that the response of their sensor based on Pd-sensitized ZnO nanostructures towards 50 ppm NH_3 is 3.4 at 100 ^oC with the response and recovery time of 20 and 60 s, respectively [3]. Although the sensor has also been tested at room temperature, its recovery time (>40 min) is quite long for the practical applications [3]. Bedi and Singh reported that the gas sensor based on the CuO film showed a respond sensitivity of 9 toward 100 ppm NH_3 at room temperature, but its signal seemed not fully recovered [41]. Hoa et al reported that a sensor based on nanocomposite of carbon nanotubes and SnO_2 showed a response time of 100 s and a recovery time of 3.2 min respectively, but the sensor only detected the concentration of NH_3 down to 10 ppm at room temperature [42]. Kshirsagar et al reported that the respond sensitivity of a ZnO films NH_3 sensor to 400 ppm of NH_3 gas is only 1.15 at room temperature with a response time of 240 s and a recovery time of 900 s, respectively [43]. The NH_3 sensor based on the network Co_3O_4 nano-sheet array in this study showed excellent sensitivity, rapid response/recovery time. It could detect the concentration of NH_3 down to 0.2 ppm at room temperature.

Fig. 10 displays the real-time transient for the NH_3 sensing of the sensor based on Co_3O_4 nano-sheets when it was exposed to 20 ppm NH_3 gas at room temperature. The response curve indicates that the sensor has a rapid response to the NH_3 gas. When the sensor was exposed to the purged air, the response of the sensor could be returned near to the baseline level. The response time and recovery time were determined to be 204 s and 835 s, respectively.

Once the Co_3O_4 nano-sheets are exposed to the air, oxygen adsorption plays an important role in electrical transport properties of the Co_3O_4 nano-sheets. At room temperature, the surface oxygen species O_2^- is the most active one [24].

$$O_{2(g)} \rightarrow O_{2(ad)} \quad (10)$$

$$O_{2(ad)} + e^- \rightarrow O_{2(ad)}^- \quad (11)$$

Surface acceptor states are created by the oxygen adsorption and trapped electrons, and in turn both the accumulation of holes and the electrical carrier concentrations are enhanced. These changes result in an increase in the conductivity of the gas sensor and the downward bending of energy band, thus producing an accumulation layer of holes [13] on the surface and generating a barrier $\Delta\phi$ as shown in Fig. 11b. It is different with the energy band in an Ar atmosphere (as shown in Fig. 11a).

When the NH_3 gas molecules contact with the oxygen species covered on the oxide surface, the reactions between the NH_3 and adsorbed oxygen are triggered based on the following chemical reactions [44]:

$$NH_3(gas) \rightarrow NH_{3ads} \quad (12)$$

$$4NH_{3ads} + 3O_2^- \rightarrow 2N_2 + 6H_2O + 3e^- \quad (13)$$

As a consequence, when the sensor is exposed to NH_3 gas, the electrons trapped by the adsorptive states will be released to combine with the holes, which results in the accumulation layer of holes reduced. Therefore the potential barrier ($\Delta\phi$) is increased as shown in Fig. 11c, leading to an increase in sensor resistance. This is opposite to

the n-type semiconductor gas sensors [45,46].

The nano-sheet surface structures are advantageous to achieve quick and significant gas responses via effective and rapid diffusion of gas onto the sensor surfaces. It can supply multiple-transportation and diffusion paths for the target gas molecules, thus enhancing gas diffusion and mass transportation through the nano-sheet sensing material. Moreover, the surface of sheets can promote the formation of more chemisorbed oxygen species. Thus, the ammonia molecules can efficiently react with the oxygen species on the sensor surface, which can change the electrical resistance significantly, thus increasing the sensitivity to the target NH_3 gas.

Apart from the high sensitivity, another important property is the reproducibility of the Co_3O_4 nano-sheets sensor. By successively exposed to the NH_3 gas with a concentration of 20 ppm for 5 cycles at room temperature, the Co_3O_4 nano-sheets based sensor shows a good reproducibility as demonstrated in Fig. 12a. During the repeated NH_3 gas injection and dry air purging processes, the response-recovery curves of the sensor are almost identical. No apparent resistance attenuation is detected after the repeated testing. It shows a stable response curve with a maximum response of 2.30 when it is exposed to 20 ppm NH_3. The response time and recovery time are almost identical for the five repeated tests, and the fluctuation of response values are less than 3%, indicating the good reproducibility characteristics of the Co_3O_4 nano-sheets based gas sensor.

Long-term stability, other critical parameters for the sensor during the practical application, has been investigated as shown in Fig. 12b. For the stability test, the

response of the gas sensor to the NH_3 was recorded once in a day for 23 days. From Fig. 10b, it can be concluded that the responses of the gas sensor are constant and the deviation of sensor's response to 100 ppm NH_3 was lower than 3% after repeated testing for 23 days, indicating that the sensor possesses an excellent long-term stability for NH_3 detection.

For practical application, the selectivity of the gas sensor is another critical parameter. A poor selectivity of a gas sensor would lead to a false alarm, thus severely limiting its industrial applications. Therefore, the sensing responses of the Co_3O_4 nano-sheets based sensor to several common reducing gases (including NH_3, H_2S, CO, H_2 and C_2H_5OH) were measured at the same gas concentration of 100 ppm at room temperature. The measurement results are shown in Fig. 13a. Clearly, the Co_3O_4 nano-sheets based sensor displays a remarkably higher response to NH_3 gas than those to other gases at the same test conditions. Fig. 13b shows the sensitivity data of the sensor exposed to the different target gases. As shown in Fig. 13b, the response sensitivity to H_2S, CO, H_2, C_2H_5OH are 2.0, 1.4, 1.2 and 1.5, respectively. These values are far less than the response sensitivity towards the NH_3 gas, which reaches 9.5 at the same concentration of 100 ppm. It means that the gas response to NH_3 was 4.65, 6.64, 7.75 and 6.20 times higher than that those to H_2S, CO, H_2, and C_2H_5OH, respectively. It suggests that the sensor has an excellent selective toward the NH_3.

4. Conclusions

In summary, network nano-sheet arrays of Co_3O_4 on alumina ceramic tube were prepared using a facile hydrothermal process without any template or surfactant. The network pristine Co_3O_4 nano-sheet array showed a uniform nano-sheet array structure

with a thickness of 39.5 nm, which is consisted of nanoparticles with an average diameter of 20 nm. Gas sensor based on the network Co_3O_4 nano-sheets array showed excellent sensitivity, rapid response/recovery time and low detection limit (0.2 ppm) towards NH_3 gas at the room temperature. Therefore, the Co_3O_4 nano-sheet array investigated in this study can be efficiently used for high-performance NH_3 gas sensor.

Acknowledgments

This work was supported by the Joint Fund of the National Natural Science Foundation of China and the China Academy of Engineering Physics (U1330108). Funding support from the UoA and CAPEX from Northumbria University at Newcastle, and Royal academy of Engineering UK-Research Exchange with China and India is also acknowledged.

Reference

[1] I.D. Kim, A. Rothschild and H.L. Tuller, Advances and new directions in gas-sensing devices, Acta. Mater. 61 (2013) 974-1000.

[2] E. Comini, C. Baratto, I. Concina, G.Faglia, M. Falasconi, M. Ferroni, V. Galstyan, E. Gobbi, A. Ponzoni, A. Vomiero, D. Zappa, V. Sberveglieri, G. Sberveglieri, Metal oxide nanoscience and nanotechnology for chemical sensors, Sens. Actuators B 179 (2013) 3-20.

[3] Y. Zeng, Z. Lou, L.L. Wang, B. Zou, T. Zhang, W.T. Zheng, G.T. Zou, Enhanced ammonia sensing performances of Pd-sensitized flowerlike ZnO nanostructure, Sens. Actuators B 156 (2011) 395-400.

[4] G.N. Dar, A. Umar, S.A. Zaidi, S. Baskoutas, S.W. Hwang, M. Abaker, A. Al-Hajry, S.A. Al-Sayari, Ultra-high sensitive ammonia chemical sensor based on ZnO nanopencils, Talanta 89 (2012) 155-161.

[5] C.N. Xu, N. Miura, Y. Ishida, K. Matsuda, N. Yamazoe, Selective detection of NH_3 over NO in combustion exhausts by using Au and MoO_3 doubly promoted WO_3 element, Sens. Actuators B 65 (2000) 163-165.

[6] C. Li, D. Zhang, B. Lei, S. Han, X. Liu, C. Zhou, Surface treatment and doping dependence of In_2O_3 nanowires as ammonia sensors, J. Phys. Chem. B 107 (2003) 12451-12455.

[7] P. Guo, H. Pan, Selectivity of Ti-doped In_2O_3 ceramics as an ammonia sensor, Sens. Actuators B 114 (2006) 762-767.

[8] A. Satsuma, K. Shimizu, T. Hattori, H. Nishiyama, S. Kakimoto, S. Sugaya, H. Yokoi, Polytungstate clusters on zirconia as a sensing material for a selective ammonia gas sensor, Sens. Actuators B 123 (2007) 757-762.

[9] V. Modafferi, G. Panzera, A. Donato, P.L. Antonucci, C. Cannilla, N. Donato, D. Spadaro, G. Neri, Highly sensitive ammonia resistive sensor based on electrospun V_2O_5 fibers, Sens. Actuators B 163 (2012) 61-68.

[10] J.R. Huang, J.H. Wang, C.P. Gu, K. Yu, F.L. Meng, J.H. Liu, A novel highly sensitive gas ionization sensor for ammonia detection, Sens. Actuators A 150 (2009) 218-223.

[11] E. Bekyarova, M. Davis, T. Burch, M.E. Itkis, B. Zhao, S. Sunshine, R.C. Haddon, Chemically functionalized single-walled carbon nanotubes as ammonia sensors, J. Phys. Chem. B 108 (2004) 19717-19720.

[12] M. Abaker, A. Umar, S. Baskoutas, G.N. Dar, S.A. Zaidi, S.A. Al-Sayari, A. Al-Hajry, S.H. Kim and S.W. Hwang, A highly sensitive ammonia chemical sensor based on α-Fe_2O_3 nanoellipsoids, J. Phys. D: Appl. Phys. 44 (2011) 425401-425407.

[13] J.N. Deng, R. Zhang, L.L. Wang, Z. Lou, T. Zhang, Enhanced sensing performance of the Co_3O_4 hierarchical nanorods to NH_3 gas, Sens. Actuators B 209 (2015) 449-455.

[14] Y. G. Li, B. Tan, Y. Y. Wu, Mesoporous Co_3O_4 nanowire arrays for lithium ion batteries with high capacity and rate capability. Nano Lett. 8 (2008) 265-270.

[15] N. Du, H. Zhang, B. Chen, J. Wu, X. Ma, Z. Liu, Y. Zhang, D. Yang, X. Huang, J. Tu, Porous Co_3O_4 nanotubes derived from $Co_4(CO)_{12}$ clusters on carbon nanotube templates: a highly efficient material for Li battery applications, Adv. Mater. 19 (2007) 4505-4509.

[16] X.W. Lou, D. Deng, J.Y. Lee, J. Feng, Archer, L. A. Self-supported formation of needlelike Co_3O_4 nanotubes and their application as lithium-ion battery electrodes. Adv. Mater. 20 (2008) 258-262.

[17] Y. Sun, P. Lv, J.Y. Yang, L. He, J.C. Nie, X.W. Liu and Y.D. Li, Ultrathin Co_3O_4 nanowires

with high catalytic oxidation of CO, Chem. Commun. 47 (2011) 11279-11281.

[18] L.F. Chen, J.C. Hu, R. Richards, S. Prikhodko and S. Kodambaka, Synthesis and surface activity of single-crystalline Co_3O_4 (111) holey nanosheets, Nanoscale 2 (2010) 1657-1660.

[19] C.W. Sun, S. Rajasekhara, Y.J. Chen and John B. Goodenough, Facile synthesis of monodisperse porous Co_3O_4 microspheres with superior ethanol sensing propertiesw, Chem. Commun. 47 (2011) 12852-12854.

[20] J.W. Yoon, J.K. Choi, J.H. Lee, Design of a highly sensitive and selective C_2H_5OH sensor using p-type Co_3O_4 nanofibers, Sens. Actuators B 161 (2012) 570-577.

[21] Q.Z. Jiao, M. Fu, C. You, Y. Zhao, H.S. Li, Preparation of hollow Co_3O_4 microspheres and their ethanol sensing properties, Inorg. Chem. 51 (2012) 11513-11520.

[22] M. M. Rahman, A. Jamal, S. B. Khan, and M. Faisal, Fabrication of highly sensitive ethanol chemical sensor based on Sm-doped Co_3O_4 nanokernels by a hydrothermal method, J. Phys. Chem. C, 115 (2011) 9503-9510.

[23] H. M. Jeong, H.J. Kim, P. Rai, J.W. Yoon, J.H. Lee, Cr-doped Co3O4 nanorods as chemiresistor for ultra selective monitoring of methyl benzene, Sens. Actuators B 201 (2014) 482-489.

[24] D. Patil, P. Patil, V. Subramanian, P.A. Joy, H.S. Potdar, Highly sensitive and fast responding CO sensor based on Co_3O_4 nanorods, Talanta 81 (2010) 37-43.

[25] C.C. Li, X.M. Yin, T.H. Wang, and H.C. Zeng, Morphogenesis of Highly Uniform $CoCO_3$ Submicrometer Crystals and Their Conversion to Mesoporous Co_3O_4 for Gas-Sensing Applications, Chem. Mater. 21 (2009) 4984-4992.

[26] L.L. Wang, J.N. Deng, Z. Lou, and T. Zhang, Cross-linked p-type Co_3O_4 octahedral

nanoparticles in 1D n-type TiO_2 nanofibers for high-performance sensing devices, J. Mater. Chem. A 2 (2014) 10022-10028.

[27] L.L. Wang, H.M. Dou, Z. Lou and T. Zhang, Encapsuled nanoreactors (Au@SnO_2): a new sensing material for chemical sensors, Nanoscale 5 (2013) 2686-2691.

[28] L.L. Wang, T. Fei, Z. Lou and T. Zhang, Three-Dimensional Hierarchical Flowerlike alpha-Fe_2O_3 Nanostructures: Synthesis and Ethanol-Sensing Properties, ACS Appl. Mater. Interfaces 3 (2011) 4689-4694.

[29] Y.G. Li and Y.Y. Wu, Critical Role of Screw Dislocation in the growth of $Co(OH)_2$ nanowires as intermediates for Co_3O_4 nanowire growth, Chem. Mater. 22 (2010) 5537-5542.

[30] P.Y. Keng, B.Y. Kim, I.B. Shim, R. Sahoo, P. E. Veneman, N.R. Armstrong, H. Yoo, J.E. Pemberton, M.M. Bull, J.J. Griebel, E.L. Ratcliff, K.G. Nebesny and J. Pyun, Colloidal polymerization of polymer-coated ferromagnetic nanoparticles into cobalt oxide nanowires, Chem. Mater. 23 (2011) 1120-1129.

[31] Y. Li, B. Tan, Y. Wu, Free standing mesoporous quasi-single-crystalline Co_3O_4 nanowire arrays, J. Am. Chem. Soc. 128 (2006) 14258-14259.

[32] H. Huang, W.J. Zhu, X.Y. Tao, Y. Xia, Z.Y. Yu, J.W. Fang, Y.P. Gan, and W.K. Zhang, Nanocrystal-constructed mesoporous single-crystalline Co_3O_4 nanobelts with superior rate capability for advanced lithium-ion batteries, ACS Appl. Mater. Inter. 4 (2012) 5974-5980.

[33] Y.Q. Fan, H.B. Shao, J.M. Wang, L. Liu, J.Q. Zhang and C.A. Cao, Synthesis of foam-like freestanding Co_3O_4 nanosheets with enhanced electrochemical activities, Chem. Commun. 47 (2011) 3469-3471.

[34] X. Wang, X.L. Wu, Y.G. Guo, Y.T. Zhong, X.Q. Cao, Y. Ma, and J.N. Yao, Synthesis and

lithium storage properties of Co_3O_4 nanosheet-assembled multishelled hollow spheres, Adv. Funct. Mater. 20 (2010) 1680-1686.

[35] Y. Wang, H. Xia, L. Lu, and J.Y. Lin, Excellent performance in lithium-ion battery anodes: rational synthesis of $Co(CO_3)_{0.5}(OH)0.11H_2O$ nanobelt array and its conversion into mesoporous and single-crystal Co_3O_4, ACS Nano 4 (2012) 1425-1432.

[36] T. He, D.R. Chen, X.L. Jiao, Y.L. Wang, and Y.Z. Duan, Solubility-controlled synthesis of high-quality Co_3O_4 nanocrystals, Chem. Mater. 17 (2005) 4023-4030.

[37] X. R, Z.H. Chun, Self-generation of tiered surfactant superstructures for one-pot synthesis of Co_3O_4 nanocubes and their close and non-close-packed organizations, Langmuir 20 (2004) 9780-9790.

[38] A. Gulino, P. Dapporto, P. Rossi, and I. Fragala, A novel self-generating liquid MOCVD precursor for Co_3O_4 thin films, Chem. Mater. 15 (2003) 3748-3752.

[39] R. Xu, J.W. Wang, Q.Y. Li, G.Y. Sun, E.B. Wang , S.H. Li, J.M. Gu, M.L. Ju, Porous cobalt oxide (Co_3O_4) nanorods: Facile syntheses, optical property and application in lithium-ion batteries, J. Solid State Chem. 182 (2009) 3177-3182.

[40] Q.Y. Yan, X.Y. Li, Q.D. Zhao, G.H. Chen, Shape-controlled fabrication of the porous Co_3O_4 nanoflower clusters for efficient catalytic oxidation of gaseous toluene, J. Hazard Mater. 210 (2012) 385-391.

[41] R.K. Bedi and I. Singh, Room-temperature ammonia sensor based on cationic surfactant-assisted nanocrystalline CuO, ACS Appl. Mater. Interfaces 2 (2010) 1361–1368.

[42] N.D. Hoa, N.V. Quy, Y.S. Cho, D. Kim, Nanocomposite of SWNTs and SnO_2 fabricated by soldering process for ammonia gas sensor application, Physica Status Solidi A 204 (2007) 1820–

1824.

[43] A. Kshirsagar, A.B. Joshi, A. Joshi, D.K. Avasthi, T.M. Bhave, S.A. Gangal, Comparative study of irradiated and annealed ZnO thin films for room temperature ammonia gas sensing, IEEE Sensors 3 (2007) 162–165.

[44] J.M. Tulliani, A. Cavalieri, S. Musso, E. Sardella, F. Geobaldo, Room temperature ammonia sensors based on zinc oxide and functionalized graphite and multi-walled carbon nanotubes, Sens. Actuators B 152 (2011) 144-154.

[45] Z.J. Li, Y.W. Huang, S.C. Zhang, W.M. Chen, Z. Kuang, D.Y. Ao, W. Liu, Y.Q. Fu, A fast response & recovery H_2S gas sensor based on α-Fe_2O_3 nanoparticles with ppb level detection limit, J. Hazard Mater. 300 (2015) 167-174.

[45] S.C. Zhang, Y.W. Huang, Z. Kuang, S.Y. Wang, W. L. Song, D.Y. Ao, W. Liu and Z.J. Li, Solvothermal synthesized In_2O_3 nanoparticles for ppb level H_2S detection. Nanosci. Nanotechnol. Lett. 7(2015) 455–461.

[46] Y.W. Huang, W.M. Chen, S.C. Zhang, Z. Kuang, D.Y. Ao, N. R. Alkurdc, W.L. Zhou, W. Liu, W.Z. Shen, Z.J. Li, A high performance hydrogen sulfide gas sensor based on porous α-Fe_2O_3 operates at room-temperature, Appl. Surf. Sci. 351 (2015) 1025-1033.

Biographies

Dr. ZhiJie Li is an associate professor in School of Physical Electronics at University of Electronic Science and Technology of China. He obtained his Ph.D degree of physical chemistry from Institute of Coal Chemistry, Chinese Academy of Sciences in 2005. His research interests include nano materials, gas sensors and surface acoustic wave (SAW) devices.

Zhijie Lin obtained his B.S. degree at North University of China in 2014. He is a graduate student in School of Physical Electronics at University of Electronic Science and Technology of China. His research interests include gas sensors and surface acoustic wave (SAW) devices.

Ningning Wang obtained her B.S. degree at Shijiazhuang University in 2014. She is a graduate student in School of Physical Electronics at University of Electronic Science and Technology of China. Her research interests include gas sensors and surface acoustic wave (SAW) devices.

Junqiang Wang obtained his B.S. degree at Yancheng Teachers University in 2015. He is a graduate student in School of Physical Electronics at University of Electronic Science and Technology of China. His research interests include applications of nanomaterials and functional thin films for sensors.

Dr. Wei Liu received his Ph.D degree of condensed matter physics in 2012 at Beihang University and he is currently an associated professor at School of Physical Electronics, University of Electronic Science and Technology of China. His one of the prime research interest is the mirostructure charaterization and analysis of nano-materials.

Dr. Kai Sun received his Ph.D degree of materials science and engineering in 1998 at Dalian University of Technology and he is currently a senior research scientist at Department of Materials Science and Engineering, University of Michigan, Ann Arbor, MI, U.S.A.. His one of the prime research interest is the scanning transimission electron microscopy (STEM) mirostructure charaterization and quansi-crystal investigations.

Dr. YongQing Fu (Richard) is a Reader in Faculty of Engineering and Environment, University of Northumbria at Newcastle, UK. He was a senior lecturer/Reader in Thin Film Centre and Physics Department in University of West of Scotland, UK, and a lecturer in Heriot-Watt University, UK. He obtained his Ph.D degree from Nanyang Technological University, Singapore in 1999, and then worked as a Research Fellow in Singapore-Massachusetts Institute of Technology Alliance, and a Research Associate in University of Cambridge. He has extensive experience in advanced thin film materials, biomedical microdevices, lab-on-chip, micromechanics, microelectromechanical systems (MEMS), sensors and microfluidics, shape memory/piezoelectric thin films and nanotechnology.

Dr. Zhiguo Wang is a professor at the University of Electronic Science and Technology of China (UESTC). He graduated from Sichuan University in China and received M.S. in condensed matter physics. He got his Ph.D. in materials physics and chemistry from UESTC. His research interests include computer modeling of the electronic, thermal, mechanical, defect and doping properties of semiconductor, electrode materials, and radiation detection materials with density functional theory (DFT) simulation, molecular dynamics (MD), DFTMD, and Monte Carlo simulation.

Figure Captions

Fig. 1 (a) Schematic gas sensor based on Co_3O_4 nano-sheet array. (b) The measurement electric circuit for the gas sensor.

Fig. 2 XRD spectra of products (a) before calcination and (b) after calcination at 350 ^oC for 2 hours in air.

Fig. 3 (a) SEM image of samples with magnification of 10000 times (inset indicates the panoramic image of the Co_3O_4 on the surface of alumina tube), (b) SEM images with magnification of 40000 times,(c) TEM image of Co_3O_4 nano-sheet (d) HRTEM image showing the crystalline framework.

Fig. 4 Pore size of distribution curves of the nano-sheet Co_3O_4 samples.

Fig. 5 XPS spectra of (a) Co 2p and (b) O 1s for Co_3O_4 nano-sheets.

Fig. 6 (a) UV–vis absorption spectra of Co_3O_4 nano-sheets (b) Optical band gap energy of Co_3O_4 nano-sheets obtained by extrapolation to $\alpha = 0$.

Fig. 7 The I-V characteristics between the two neighboring electrodes bridged by the Co_3O_4 nano-sheets at room temperatures.

Fig. 8 (a) Dynamic response-recovery curve and (b) Response sensitivity of the Co_3O_4 nano-sheets based sensor to NH_3 gas at the room temperature.

Fig. 9 Response time and recovery time of the Co_3O_4 nano-sheets based sensor to NH_3 gas at the room temperature.

Fig. 10 Real-time gas sensing transients of the sensor based on Co_3O_4 nano-sheets to 20 ppm NH_3 gas at room temperature.

Fig. 11 Band diagrams and schematic images of the surface reactions at different

surroundings: (a) in Ar atmosphere, (b) exposed in air, (c) in the presence of NH_3 gas.

Fig. 12 (a) Reproducibility to 20 ppm NH_3 gas and (b) Long-term stability to 100 ppm NH_3 gas of the gas sensor based on Co_3O_4 nano-sheets at room temperature.

Fig. 13 (a) Response and (b) Sensitivity histogram of Co_3O_4 nano-sheets gas sensor towards different gases at the same concentration of 100 ppm.

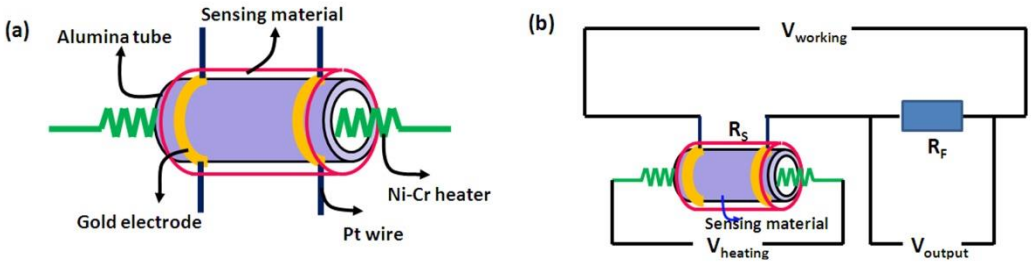

Fig. 1 (a) Schematic gas sensor based on Co_3O_4 nano-sheet array. (b) The measurement electric circuit for the gas sensor.

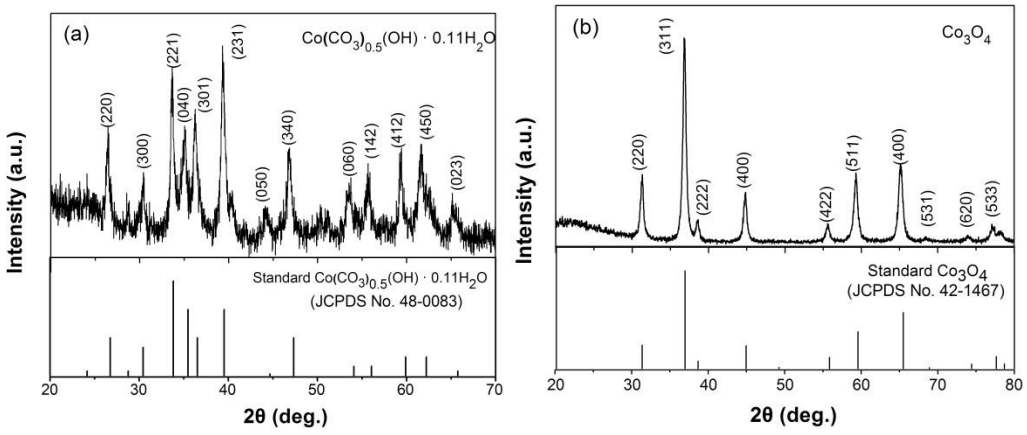

Fig. 2 XRD spectra of products (a) before calcination and (b) after calcination at 350 ^oC for 2 hours in air

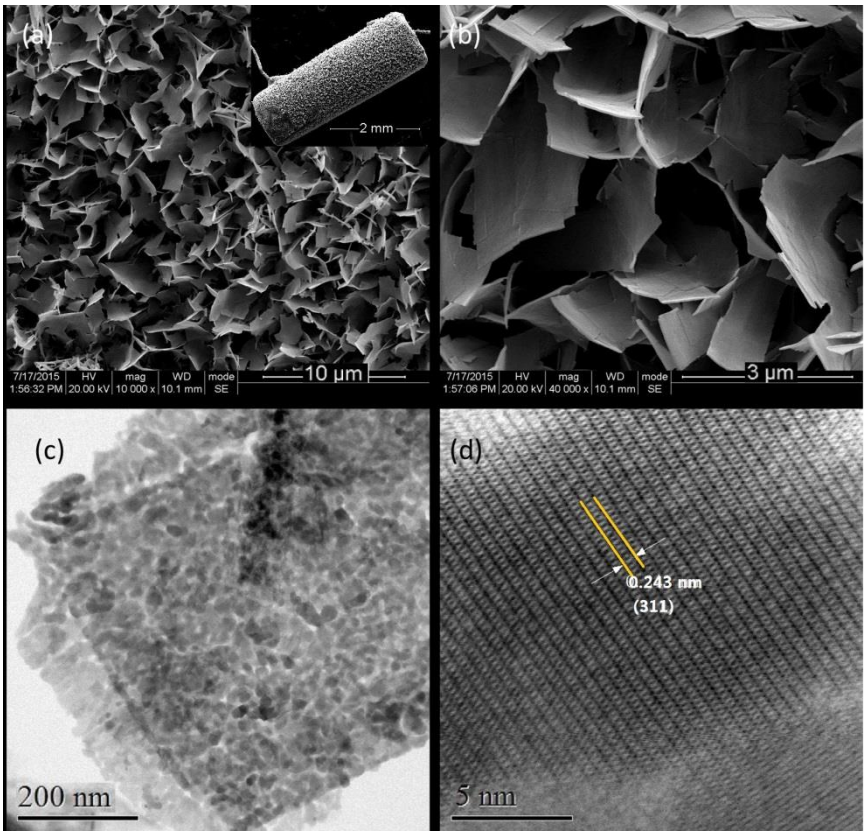

Fig. 3 (a) SEM image of samples with magnification of 10000 times (inset indicates the panoramic image of the Co_3O_4 on the surface of alumina tube), (b) SEM images with magnification of 40000 times,(c) TEM image of Co_3O_4 nano-sheet (d) HRTEM image showing the crystalline framework.

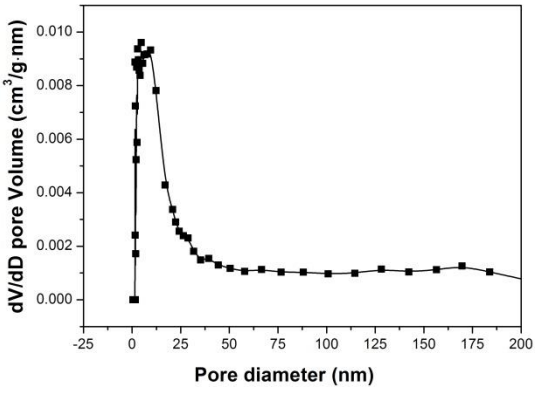

Fig. 4 Pore size of distribution curves of the nano-sheet Co_3O_4 samples using the Barrett-Joyner-Halenda (BJH) method.

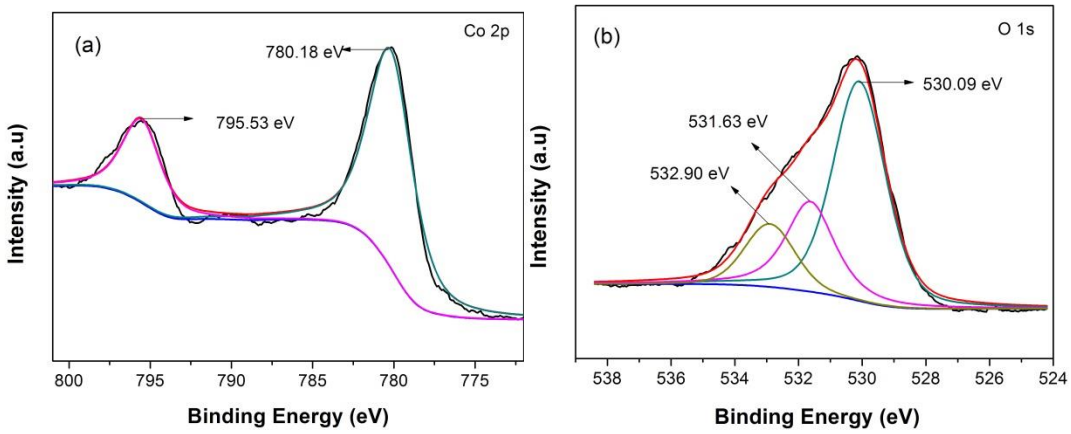

Fig. 5 XPS spectra of (a) Co 2p and (b) O 1s for Co_3O_4 nano-sheets

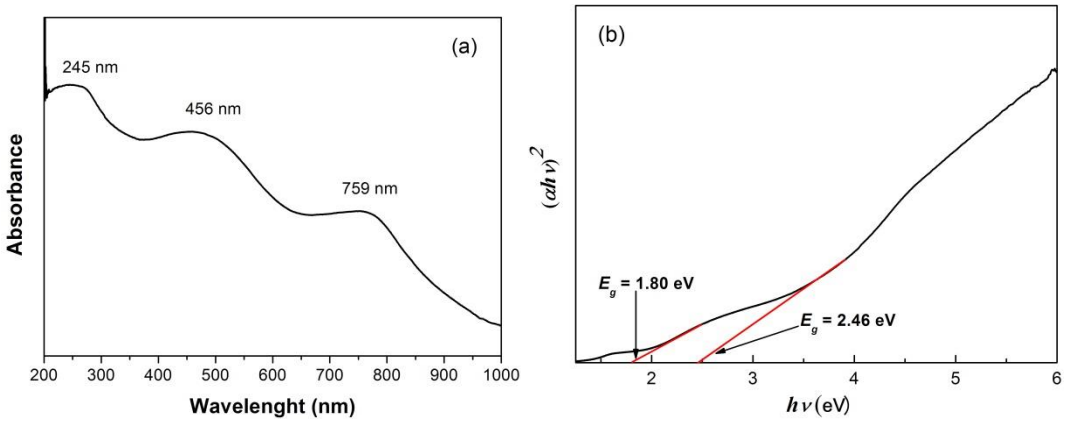

Fig. 6 (a) UV–vis absorption spectra of Co_3O_4 nano-sheets (b) Optical band gap energy of Co_3O_4 nano-sheets obtained by extrapolation to $\alpha = 0$.

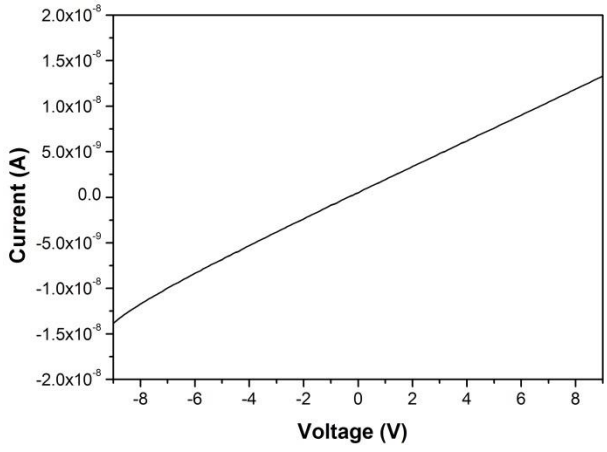

Fig. 7 The I-V characteristics between the two neighboring electrodes bridged by the Co_3O_4 nano-sheets at room temperatures

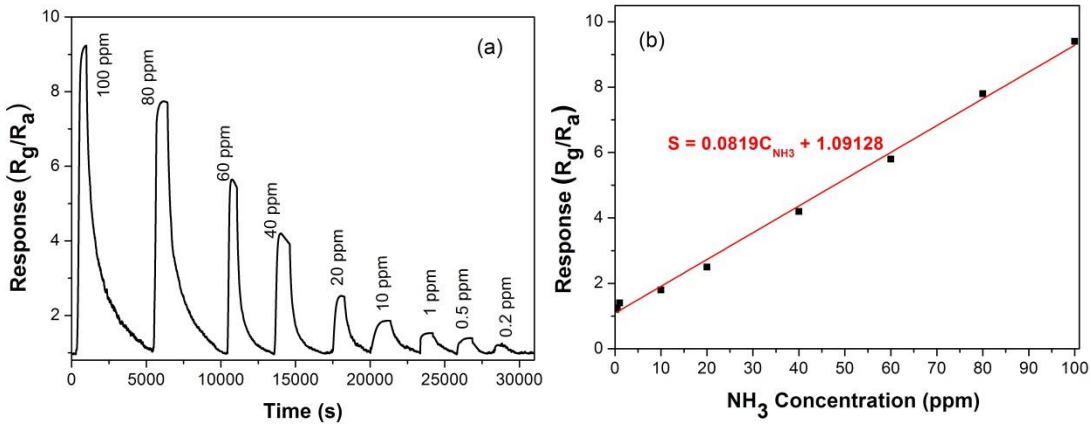

Fig. 8 (a) Dynamic response-recovery curve and (b) Response sensitivity of the Co_3O_4 nano-sheets based sensor to NH_3 gas at the room temperature.

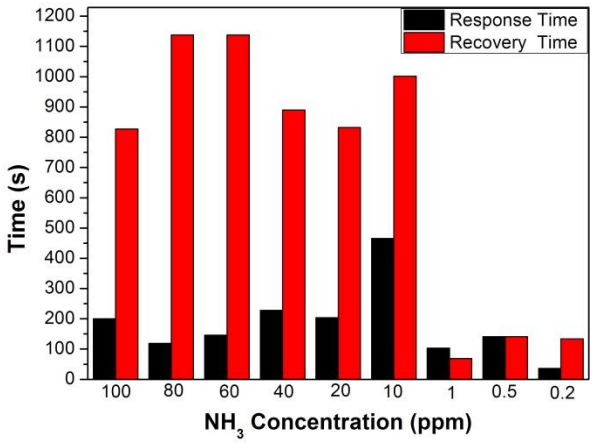

Fig. 9 Response time and recovery time of the Co_3O_4 nano-sheets based sensor to NH_3 gas at the room temperature.

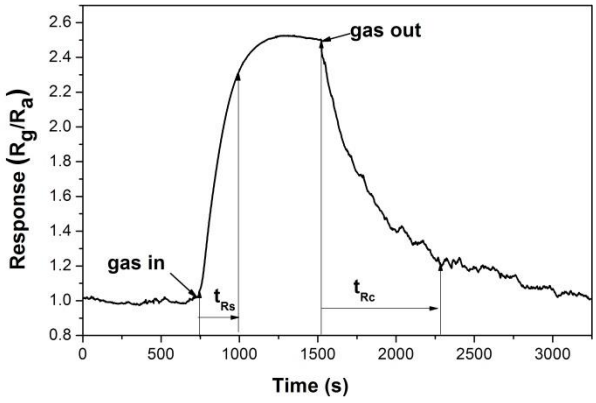

Fig. 10 Real-time gas sensing transients of the sensor based on Co_3O_4 nano-sheets to 20 ppm NH_3 gas at room temperature.

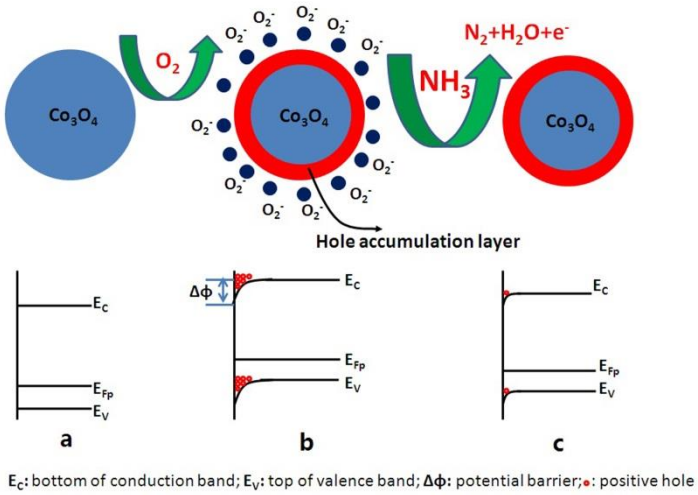

Fig. 11 Band diagrams and schematic images of the surface reactions at different surroundings: (a) in Ar atmosphere, (b) exposed in air, (c) in the presence of NH_3 gas.

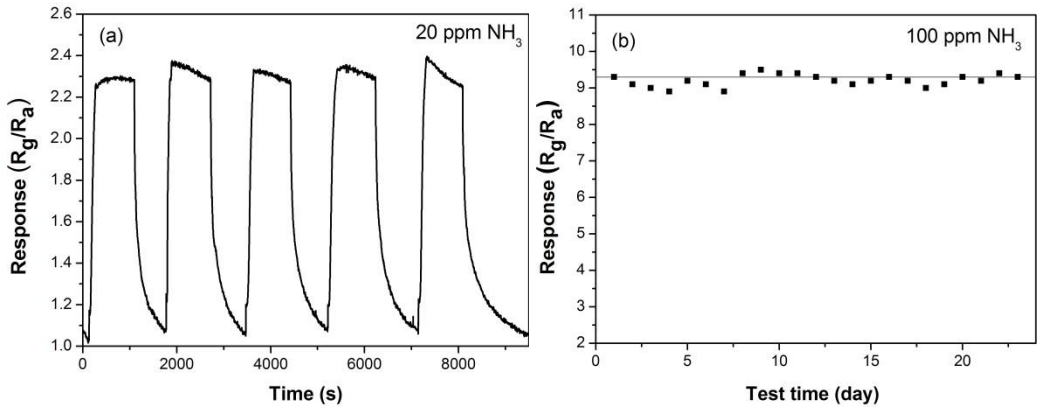

Fig. 12 (a) Reproducibility to 20 ppm NH_3 gas and (b) Long-term stability to 100

ppm NH_3 gas of the gas sensor based on Co_3O_4 nano-sheets at room temperature

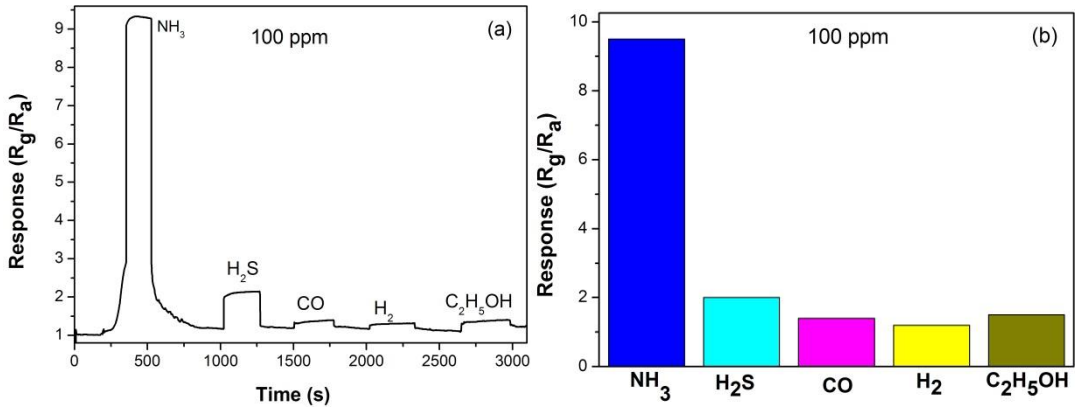

Fig. 13 (a) Response and (b) Sensitivity histogram of Co_3O_4 nano-sheets gas sensor towards different gases at the same concentration of 100 ppm.